Eur. J. Biochem. **260**, 176–182 (1999) © FEBS 1999

Crystal structure of a hybrid between ribonuclease A and bovine seminal ribonuclease – the basic surface, at 2.0 Å resolution

Efstratia H. Vatzaki,[1] Simon C. Allen,[1] Demetres D. Leonidas,[1] Katrin Trautwein-Fritz,[2] Joseph Stackhouse,[2] Steven A. Benner[2,3] and K. Ravi Acharya[1]

[1]*Department of Biology and Biochemistry, University of Bath, UK;* [2]*Department of Chemistry, Swiss Federal Institute of Technology, Zürich, Switzerland;* [3]*Division of Biochemistry, Department of Chemistry, University of Florida, Gainesville, USA*

A variant of bovine pancreatic ribonuclease A has been prepared with seven amino acid substitutions (Q55K, N62K, A64T, Y76K, S80R, E111G, N113K). These substitutions recreate in RNase A the basic surface found in bovine seminal RNase, a homologue of pancreatic RNase that diverged some 35 million years ago. Substitution of a portion of this basic surface (positions 55, 62, 64, 111 and 113) enhances the immunosuppressive activity of the RNase variant, activity found in native seminal RNase, while substitution of another portion (positions 76 and 80) attenuates the activity. Further, introduction of Gly at position 111 has been shown to increase the catalytic activity of RNase against double-stranded RNA. The variant and the wild-type (recombinant) protein were crystallized and their structures determined to a resolution of 2.0 Å. Each of the mutated amino acids is seen in the electron density map. The main change observed in the mutant structure compared with the wild-type is the region encompassing residues 16–22, where the structure is more disordered. This loop is the region where the polypeptide chain of RNase A is cleaved by subtilisin to form RNase S, and undergoes conformational change to allow residues 1–20 of the RNase to swap between subunits in the covalent seminal RNase dimer.

Keywords: crystal structure; molecular evolution; ribonuclease; site-directed mutagenesis; X-ray crystallography.

New biomolecular function has arisen during the divergence of the ribonuclease (RNase) superfamily of proteins over the past 300 million years through repeated gene duplication [1] and natural selection [2], starting at least as early as the time when the first animals appeared on land. In contemporary mammals, the RNase superfamily includes proteins such as angiogenin [3,4], eosinophil-derived neurotoxin and eosinophil cationic protein [5,6]. In the amphibian, the superfamily is represented by the P-30 protein (onconase) from frog eggs, which has antitumour activity [7], and a sialic acid-binding lectin from frog [8].

One member of the RNase superfamily has emerged very recently in the seminal plasma of ruminants. Although the seminal RNase gene family arose by duplication of the pancreatic gene some 35 million years ago [9], only in organisms diverging within the past few million years it is expressed as active protein [2]. In the past few million years, it has undergone an enormously rapid evolution in sequence, characteristic of a protein under selection to perform a new role.

Originally isolated by D'Alessio [10], seminal RNase displays antiproliferative activity [11,12], immunosuppressive activity [13–15], antispermatogenic activity [16], and affinity for anionic glycolipids such as gangliosides and seminolipid (N. Trabesinger-Rüf and S. A. Benner, unpublished results). Each of these activities essentially absent from pancreatic RNase and from the most recent common ancestor of seminal and pancreatic RNase. Thus, these traits are all recently derived.

Bovine seminal RNase (BS-RNase) is also interesting as a structurally unique example of a homodimeric protein joined by two intersubunit disulphide bonds [17]. These are formed between Cys31 of one subunit and Cys32 of the other [18]. Further, the active sites of the seminal RNase homodimer are composite. One of the essential histidine residues (His12) comes from the peptide segment 1–20 which is swapped with an identical peptide segment of the other subunit. Finally, one surface of seminal RNase is remarkably basic, with seven neighbouring positive charges and no compensating negative charges on one face of the protein.

Considerable amounts of experimental data have identified amino acid substitutions that confer dimer structure [19–21], binding and catalytic activity against duplex RNA [22], and immunosuppressivity (J. Soucek and S. A. Benner, unpublished data) upon pancreatic-type ribonucleases. Each of these properties of seminal RNase can be localized in a defined set of amino acid substitutions. In most cases, residues that contribute to dimeric structure are involved, and dimeric structure has been the focus of most work in seminal RNase to date [23,24], in part because the impact on the three-dimensional structure is obvious.

However, other studies [22] have identified a second set of amino acids that are relevant to all of these properties, although in a different way. These residues form a basic surface in seminal RNase, with Lys replacing Gln55, Asn62, Tyr76, and Asn-113 in pancreatic RNase, Arg replacing Ser80, Thr replacing Ala64 and Gly replacing Glu111. The impact of these amino acid substitutions on the overall fold of the structure is not so clear.

In order to understand how the 'basic surface' might influence

Correspondence to K. R. Acharya, Department of Biology and Biochemistry, South Building, University of Bath, Claverton Down, Bath BA2 7AY, U.K. Tel. + 44 1225 826 238. Fax: + 44 1225 826 779. E-mail: K.R.Acharya@bath.ac.uk

Abbreviations: BS-RNase, bovine seminal RNase.

(Received 22 September 1998, revised 17 November 1998, accepted 24 November 1998)

the three-dimensional structure of a protein, we have prepared a hybrid that introduces the entire basic surface alone from seminal RNase into a RNase background. The variant **A**(Q55K, N62K, A64T, Y76K, S80R, E111G, N113K) was crystallized and the crystal structure determined at 2.0 Å resolution. The structure is reported here. Also, we report the structure of wild-type RNase A (recombinant protein) at 2.0 Å resolution.

MATERIALS AND METHODS

Preparation of proteins

The variant **A**(Q55K, N62K, A64T, Y76K, S80R, E111G, N113K) presenting the complete basic surface of seminal RNase in an RNase A background was constructed in three steps via three intermediate variants **A**(Q55K, N62K, A64T), **A**(Y76K, S80R) and A(E111G, N113K), each beginning with a synthetic gene for RNase A into which had been engineered unique restriction sites [25] manipulated within the pUC vector [26]. Variant **A**(Q55K, N62K, A64T) was prepared by replacing a DNA fragment between the *Hpa*I and *Bal*I sites (codons 44–70) with a synthetic fragment containing the desired codons. Variant **A**(Y76K, S80R) was prepared by replacing a DNA fragment between the *Bal*I and *Pst*I sites (codons 70–83) with another synthetic fragment containing the desired codons. Variant (E111G, N113K) was analogously prepared by replacing a DNA fragment between the *Hha*I and *Bam*HI sites (codons 96–124) with a synthetic fragment containing the desired codons. Variant **A**(Q55K, N62K, A64T, Y76K, S80R, E111G, N113K) was constructed by a four-part ligation joining the pUN2 plasmid containing RNase [27] digested with *Xho*I and *Bam*HI and the *Xho*I–*Bal*I fragment from the first variant, the *Bal*I–*Pst*I fragment from the second, and the *Pst*I–*Bam*HI fragment from the third. The constructed plasmid was used to transform lon-cells, which were then grown on enriched LB medium (1 L) to an optical density of 1.2 (550 nm). Expression was initiated by heat shock (42 °C), and allowed to proceed for 2.5 h. Cells were harvested by centrifugation (15 min, 60 000 ***g***). The cell paste was diluted with 4 vol. of lysis buffer (Tris base, 50 mM, NaCl 50 mM, ethylenediaminetetra(acetic acid) (EDTA) 10 mM, phenylmethanesulphonylfluoride 0.1 mM, pH adjusted with diluted HCl to 8.0), and the cells lysed in a French press (two passes, 11 000 p.s.i.). The mixture was centrifuged (10 min, 6000 ***g***), the supernatant discarded, and the pellet suspended in 9 vol. of Tris buffer (50 mM, pH 7.8, NaCl 100 mM, EDTA 10 mM, sarcosine 40 mM, phenylmethanesulphonylfluoride 0.1 mM, 2-mercaptoethanol 100 mM) containing urea (8 M). The mixtures was shaken (30 °C, 2 h), and then diluted slowly with 9 vol. of buffer as above, but lacking urea and containing oxidized (1 mM) and reduced (10 mM) glutathione. The mixture was incubated (4 °C, 4–12 h) and centrifuged (15 min, 6000 ***g***). The supernatant contained soluble variant RNase ≈70% pure. The buffer was exchanged by gel filtration (G-25, column pre-equilibrated with sodium acetate, 100 mM, pH 5.0). The protein was further purified by affinity chromatography on pUp agarose (Sigma) and assayed for catalytic activity using UpA as previously described [28]. Recombinant RNase A was expressed in *Escherichia coli* and purified as reported [25].

Protein crystallization and diffraction measurements

The recombinant RNase A was crystallized using the hanging drop vapour diffusion method. The drops (volume 6 μL) contained 10 mg·mL^{-1} protein in 10 mM sodium citrate buffer (pH 5.5) and 10% w/v poly(ethylene glycol) 4000, equilibrated against the reservoir buffer containing 20% w/v poly(ethylene glycol) 4000 and 20 mM sodium citrate buffer (pH 5.5) and placed at 16 °C. The crystals belong to the monoclinic space group C2 with cell dimensions a = 101.3 Å, b = 33.3 Å, c = 73.8 Å and β = 90.04°. These cell dimensions are very similar to those reported for native bovine pancreatic RNase A [29]. There are two RNase molecules per asymmetric unit.

The RNase variant was also crystallized from hanging drops using the vapour diffusion method. The protein was dialysed against water immediately before the crystallization trials. Three microlitres of the protein solution (final concentration in the drop 10 mg·mL^{-1}) were mixed with 3 μL of the reservoir buffer which contained 0.3 M ammonium acetate, 25% (w/v) poly(ethylene glycol) 3350 and 100 mM sodium citrate at pH 4.3, 0.02% (v/v) sodium azide and placed at 16 °C. It was observed that pH fluctuations dramatically affected the crystal formation. Crystals appeared after 1–2 days and reached their final size within 15 days. In the majority of cases, the crystals grew as long thin needles, but on occasions, the crystals were shorter and grew in the other two dimensions as well, to a maximum size of 0.4 × 0.15 × 0.1 mm. These were appropriate for X-ray diffraction studies. These crystals belong to the monoclinic $P2_1$ space group with cell dimensions a = 29.02 Å, b = 75.66 Å, c = 53.93 Å and β = 101.15°, having two molecules per asymmetric unit and 41% of the crystal volume occupied by solvent.

Diffraction data were collected on stations PX 9.6 and 7.2 of the Synchrotron radiation source (Daresbury, UK) at 2.0 Å resolution using a 30-cm-diameter MAR-Research image plate for both the wild-type and variant crystals. Low resolution data (at 2.6 Å) for the RNase variant were collected using the in-house Siemens area detector mounted on a Siemens rotating anode X-ray source with CuKα radiation operating at 45 kV and 80 mA.

Data processing and phase calculation

Raw data images from the synchrotron dataset were indexed, integrated and corrected for Lorentz and polarization effects using the program DENZO [30]. All data were scaled and merged using the program SCALEPACK [30]. The program XDS [31] was used for data processing and reduction of the low resolution in-house area detector data. The two datasets were merged and scaled by the SCALA program [32]. Intensities were truncated to amplitudes by the program TRUNCATE [33]. The details of data processing statistics are presented in Table 1. Both structures were determined by the molecular replacement method using the program AMoRe [34] with the coordinates of native RNase at 1.45 Å resolution (PDB-3RN3 [35]). The positions of the two molecules in the asymmetric unit for both structures were determined using data in the ranges of 10–3.5 Å in rotation and translation function searches.

Refinement

The output models from AMoRe were subjected to rigid-body refinement with X-PLOR [36] using data from 10 to 2.5 Å for the recombinant RNase. The R_{free} [37] at this stage was 36.3% and the conventional R_{cryst} 35.6%. For variant RNase, data from 10 to 2.6 Å were initially used in rigid-body refinement, the R_{free} was 30.0% and the conventional R_{cryst} 28.0%. Alternating cycles of manual building, conventional positional refinement and the simulated annealing method as implemented in X-PLOR 3.851 improved the models, while solvent correction as implemented in X-PLOR 3. 851 [38] allowed the inclusion of low resolution data from 20 Å. Extension of the refinement

Table 1. X-ray data collection and refinement statistics.

	Recombinant RNase A	RNase variant
Data collection statistics		
Resolution (Å)	25–2.0	25–2.0
Reflections measured	21154	29658
Unique reflections	14022	16566
Completeness (outer shell) (%)	82.4 (74.7)	96.5 (89.7)
I/σ(I)	6.3	6.2
Multiplicity	1.5	1.8
R_{sym}[a] (%)	9.0	9.7
Refinement statistics		
Resolution (Å)	20–2.0	20–2.0
R_{cryst}[b] (%)	19.1	18.2
R_{free}[c] (%)	25.9	25.6
Number of reflections	13957	15037
Number of protein atoms	1902	1904
Number of water molecules	109	102
Deviations from ideality (r.m.s.)		
Bond lengths (Å)	0.011	0.010
Bond angles (°)	1.6	1.5
Dihedrals (°)	27.5	27.7
Impropers (°)	0.8	0.7
Average B factor (Å^2)		
Main chain atoms	28.7	17.1
Side chain atoms	30.1	19.8
All protein atoms	29.4	18.4
Solvent atoms	43.9	35.6

[a]$R_{sym} = \Sigma_h\Sigma_i 1/2I(h) - Ii(h)1/2/\Sigma_h\Sigma_i Ii(h)$, where $Ii(h)$ and $I(h)$ are the *ith* and the mean measurements of the intensity of reflection h.[b]$R_{cryst} = \Sigma_h 1/2F_o - F_c 1/2\Sigma_h F_o$, where F_o and F_c are the observed and calculated structure factor amplitudes of reflection h, respectively.[c]R_{free} is equal to R_{cryst} for a randomly selected 5% subset of reflections not used in the refinement [37].

procedure from 2.5 to 2.0 Å resolution for the recombinant RNase A and from 2.6 to 2.0 Å for RNase variant, following the insertion of the mutated residues, was performed in 0.2 Å steps. The quality of the model was monitored using sigma A-weighted 2|**F***o*| – |**F***c*|ϕcalc maps calculated using the program SIGMAA [39]. During the final stages of refinement, water molecules (temperature factor less than 65 Å^2) were included in the model where the peaks in the |**F***o*| – |**F***c*| electron density maps appeared with heights greater than 3 σ. Tight non-crystallographic symmetry restraints were applied for both structures throughout the refinement procedure and were gradually released in the final cycle of refinement. The details for the refinement statistics are shown in the Table 1. The program PROCHECK [40] was used to check the quality of the final structures. Analysis of the Ramachandran (ϕ–ψ) plot for both structures showed that all residues lie in the allowed regions except Ser 22, due to its poor electron density and hence disordered. Figures were drawn by MOLSCRIPT [41] modified by R. Esnouf [42]. The atomic coordinates for the variant RNase molecule have been deposited with the Brookhaven Protein Data Bank (PDB code 1B6V).

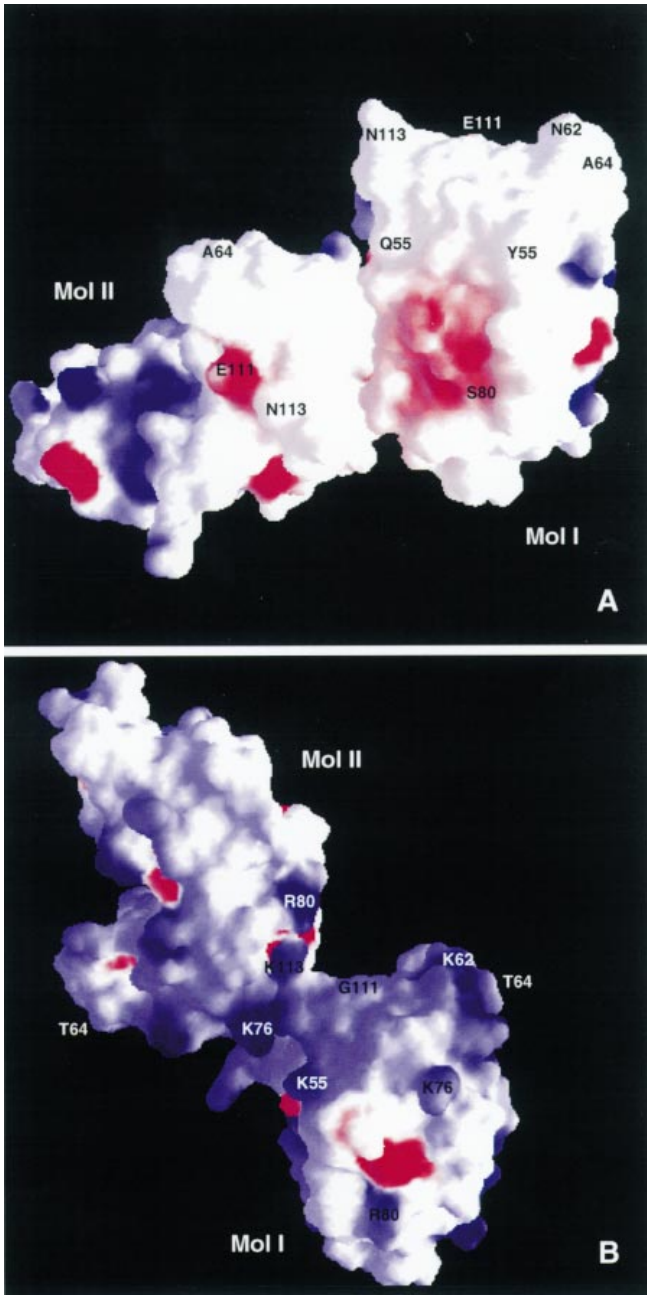

Fig. 1. Surface representation of wild-type RNase A (A) and the variant (B) dimers in the crystallographic asymmetric unit. The surfaces are coloured according to electrostatic potential from electronegative to electropositive by a red-to-blue continuous colour range. The views of mol I in both figures are almost identical: view in (B) shows the 'basic surface' in the variant and the view in (A) shows the corresponding surface in the wild-type RNase A molecule. Figure was generated using GRASP [44] with a probe radius of 1.4 Å.

RESULTS

Overall structures

The structures of recombinant RNase A and that of the RNase variant reported here are very similar to the high resolution structure of RNase A from monoclinic crystals reported previously (pdb entry 1AFU [29]), which also has two protein molecules in the asymmetric unit. The crystal packing in the recombinant RNase A is identical to 1AFU RNase A with the two monomers related by a rotation angle of ≈125° (Fig. 1A). The interface consists of residues 6–34 of one molecule and residues 50–61 and 74–78 of the other. The r.m.s. deviation on the positions of the C^α atoms for the two RNase structures (1AFU and present structure) is 0.41 Å.

The packing of the two variant RNase molecules in the asymmetric unit is quite different from that of the recombinant RNase A and the variant crystallizes in a different space group

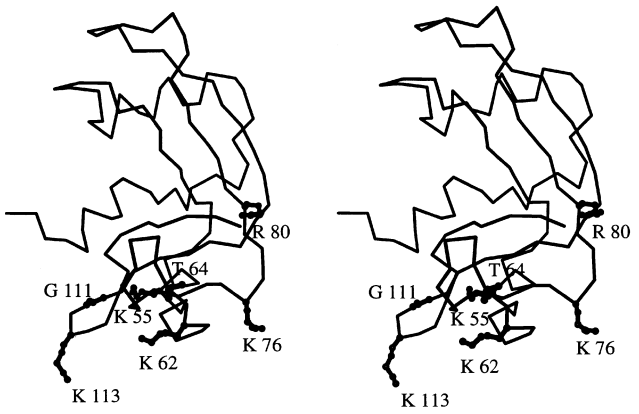

Fig. 2. Stereoview of the C^{α} backbone for the variant RNase molecule. Side chains of the mutated residues are shown as ball-and-stick models.

($P2_1$ instead of C2). Interestingly, the association of the two variant molecules resembles that of BS-RNase A dimer [18], both have a twofold molecular symmetry with a rotation angle of 180° (Fig. 1B). However, in the BS-RNase structure the dimer interface is formed by the packing of two helices (residues 22–37) in parallel, one from each molecule, while in the variant it is formed by two loops – residues 1–3 and 111–115 from one molecule, a helix (residues 50–62) and another loop (residues 78–75) from the other. There are seven water molecules at the interface between the two molecules in the recombinant structure and two of them mediate interactions between the two RNase molecules. In the variant RNase structure, the interface consists of some 10 water molecules and two of them mediate interactions between the two protein molecules.

Comparison between variant and recombinant RNases

The structures for RNase and the mutation sites for the basic surface variant **A**(Q55K, N62K, A64T, Y76K, S80R, E111G, N113K) are illustrated in Figs 1 and 2. The r.m.s. deviation for the positions of the C^{α} atoms between the two molecules in the asymmetric unit is 0.46 and 0.31 Å. Molecule I of RNase superimposes with individual molecules I and II of the variant with an r.m.s. deviation (C^{α} atoms) of 0.44 and 0.53 Å, respectively. The corresponding values for molecule II of RNase are 0.41 and 0.45 Å, respectively. All superpositions were performed using the program SHP [43]. The observed changes associated with the individual amino acid substitutions are recorded in Table 2.

The most noticeable change from the wild-type structure is in the loop regions containing residues 16–22. Very poor density is seen for these residues; in the final model positions are assigned to these atoms corresponding to their counterparts in the wild-type structure. The temperature factors (B-factors) for these residues are much higher than for the rest of the protein and this protein segment (in the variant) is not involved in any packing contacts. This change can be accounted for by assigning importance to the interaction between the side chain hydroxyl group of Ser 80 and the backbone carbonyl of Ser 18 in the wild-type structure. The introduction of an Arg at position 80 disrupts this interaction. As a consequence, the loop containing residues 16–22 is allowed to move. Furthermore, the mutation to Arg in the variant also disrupts the hydrogen bond to Nε2 of Gln 101 (Table 3). On the other hand the side chain of Arg 80 in the variant forms a new hydrogen bond with the carbonyl oxygen of His-48, which lies in the adjacent β-strand in the β-sheet that is central to the structural element of RNase (Table 3). In the nearby residue 76, the side chain in the variant is also more flexible.

A second notable change occurs at positions 111–113. For residue 113, clear density is observed for RNase, but not for the variant. Substitution at this residue is known from earlier work [22] to have a significant influence on the protein's ability to bind and melt duplex DNA and to catalyse the hydrolysis of duplex RNA.

Finally, in the first basic segment involving residues 55, 62 and 64, new side chain contacts are made in the variant. The side chain of Gln55 in the wild type does not form any hydrogen bonds; the Lys at this position in the variant forms a hydrogen bond with the side chain of Ser89. The overall charge of the variant due to the mutation of seven surface residues in RNase has changed from 3.0 to 10.0 as calculated using the program GRASP [44] (Fig. 1).

Comparison with BS-RNase

BS-RNase is a homodimer composed of two molecules T and B with an extensive interchain T/B interaction and each monomer consists of two segments T1, T2 and B1, B2 [18]. Molecules I and II of the RNase variant superimpose on to the structure of BS-RNase (1.9 Å resolution, pdb accession code 1BSR [18]) with an r.m.s. deviation (for C^{α} positions) of 0.99 Å and 0.94 Å on to segment T1/B2; 0.49 Å and 0.45 Å on to segment T2/B1, respectively (excluding the hinge peptide residues 14–21).

Table 2. Structural details at the mutation sites in the variant RNase molecule.

Mutation	Observations
Q55K	Gln55 and Lys55 are well defined within the electron density maps of the respective structures, in both molecules. Their side chains have similar orientations.
N62K	Asn62 is well defined in the electron density map in both molecules of the asymmetric unit in RNase A. Lys62 is well defined in the electron density map in molecule II but there is no density beyond atom Cδ in molecule I of the variant. The side chains of both residues in RNase and in variant point in the same direction.
A64T	The side chains are ordered in both structures. The positions of the Cβ atoms are almost identical.
Y76K	Tyr 76 is well defined in the map in RNase A while there is no density beyond Cγ in both molecules of the variant for Lys76. Their side chains point in opposite directions and the distance between atom Cγ of Tyr76 and Cγ of Lys76 is 1.2 and 1.8 Å in molecules I and II, respectively.
S80R	All the atoms of Ser 80 are well defined in the electron density map of the RNase structure. There is no density beyond atom Nε of Arg 80 in the electron density map in molecule II, while all atoms of Arg80 are well defined in the map in molecule I of the variant. The side chains of both residues, Ser in the native and Arg in the variant, point in the same direction.
E111G	Both residues are well defined in the electron density map of the respective structures.
N113K	Asn 113 is well defined in the electron density map. The position of Lys 113 in the structure of the variant is also well defined for molecule I, but there is no density beyond atom Cβ in molecule II. The side chains point in different directions and the distance between atoms Oδ1 of Asn113 (in RNase) and Nζ of Lys113 is 3.2 Å in molecule I (in the variant).

Table 3. Hydrogen bond interactions involving the side chain atoms of the mutated residues in the variant and the wild type RNase A molecules.

			Molecule I		Molecule II	
Wild type	Variant	RNase atom	Wild type	Variant	Wild type	Variant
	Lys 55 Nζ	Ser 89 Oγ[a]	–	–	–	2.4
Asn 62 Nδ2	Lys 62 Nζ	Thr 70 O	3.0	3.1	2.6	2.5
Asn 62 Nδ2		Cys 72 O	2.9	–	2.8	–
Asn 62 Oδ1		water	–	–	3.2	–
Tyr 76 Oη		water[a]	2.9	–	2.9	–
Tyr 76 Oη		water	–	–	2.8	–
Ser 80 Oγ		Ser 18 O	2.8		3.0	
Ser 80 Oγ		Gln 101 Nε2	3.0		2.7	
	Arg 80 Nη1	His 48 O		3.0		–
Glu 111 Oε1		Tyr 115 Oη[a]	–		2.4	
Glu 111 Oε2		water	–		3.0	
Lys 113 Nζ		water	–			2.5

[a] Residues from a symmetry related molecule.

Exclusion of the loop 65–72 from structural comparisons with segment B2 (which is involved in crystal packing interactions in the structure of BS-RNase) reduces r.m.s. deviation values (for C^{α} positions) with segment T1/B2–0.47 Å and 0.41 Å for molecules I and II of the variant RNase. The side chain of Lys 55 in the variant structure is involved in a crystal packing contact through a hydrogen bond (Table 3), the corresponding residue in BS-RNase structure has very similar conformation, but not involved in any interaction. Atom Nζ of Lys62 makes a hydrogen bond with the carbonyl oxygen of Thr70 in both proteins. The side chains of Thr64 and Lys76 that are not involved in hydrogen bond interactions have similar conformations in both structures. The side chains of Arg80 and Lys113 as well as the backbone of Lys113 have different conformations from their structural counterparts in the BS-RNase structure. Arg80 makes a hydrogen bond with the carbonyl oxygen of His48 in the variant structure while in BS-RNase in molecule T, it is involved in a water-mediated interaction with the side chain of Glu103 and in molecule B makes a hydrogen bond with the carbonyl oxygen of Gly116. Also the backbone conformation of Gly111 is almost identical in both proteins.

DISCUSSION

Substitutions in the basic surface of RNase have been observed to have a variety of impacts on the catalytic and biological behaviour of RNase variants [21,22]. Variant **A**(Q55K, N62K, A64T, Y76K, S80R, E111G, N113K) had a 3.6–3.8 increase in activity against double-stranded nucleic acid compared with RNase A while it had a similar activity against UpA [22]. However, this increase can be attributed to a single substitution (E111G) as variant **A**(E111G) displays the same increase in the catalytic activity against double-stranded RNA [22]. Nevertheless, both variants are ≈7 times less active than BS-RNase. The variants **A**(Q55K, N62K, A64T) and **A**(E111G, N113K) have increased immunosuppressivity (J. Soucek and S. A. Benner, unpublished results). Finally, substitutions at positions 76 and 80 destroy immunosuppressive activity created by substitutions elsewhere on the basic surface. Thus, variant **A**(Y76K, S80R) has less immunosuppressivity than pancreatic RNase A (J. Soucek and S. A. Benner, unpublished data). All of these effects are observed in mutants that do not have an increased propensity to form dimeric structure. In particular, each of these proteins is a monomer with no detectable dimer formation under native conditions.

These results provide an alternative to the view that has emerged recently [19,23], namely that the focus of biological activity is on quaternary structure: in particular, dimeric structure in RNase variants, and in the dimers, on the ability of the subunits to swap the first 20 residues to form composite active sites. With the emergence of a high resolution structure of the seminal RNase dimer [18], much structural information is available concerning the geometrical features of the dimer structure and the peptide segment 1–20 swap. Also recently, the crystal structure of an RNase A dimer with the N-terminal helix of each subunit swapped has been determined [45]. However, this RNase dimer [45] displays a totally different dimer association from those of BS-RNase and the RNase variant **A** reported here. It does not have any of the biological properties attributed to BS-RNase or to variant **A**. On the other hand variant **A**(Q55K, N62K, A64T, Y76K, S80R, E111G, N113K) has higher activity against duplex RNA than pancreatic RNase A, but without forming any of the dimeric structure characteristic of BS-RNase. The structure of the variant, in agreement with biochemical studies [22], supports the view that dimer association and catalytic activity against duplex RNA are not strongly related. Furthermore, the substitutions in the 'basic surface' do not have any effect in the catalytic site of the variant, which has an identical configuration to the site in native RNase A and hence the variant displays similar activities to RNase A against small substrates [22].

The native structure of RNase A determined some years ago [46] contained a hydrogen bond between residue 80, nominally in the basic surface, and Ser18 in the loop connecting segments 1–20. Substitution at position 80 destroys this contact, as expected. Unexpected is the consequence of this destruction, a greatly increased flexibility in the loop connecting this protein segment with the remainder of the protein (J. Soucek and S. A. Benner, unpublished results). The correlation between this contact and immunosuppressivity is not direct. This hydrogen bond is also absent in BS-RNase, which has high immunosuppressivity [18]. Most trivially, it may be that the increased flexibility of the polypeptide chain in the mutant renders it more susceptible to proteolysis. More rapid proteolytic degradation of the mutant would make it appear to be less immunosuppressive than BS-RNase in a standard mixed lymphocyte culture assay.

It is interesting to speculate that the effect might be reciprocal. Alteration in the amino acid sequence of the loop might also destroy the main chain backbone interaction between Ser18 and Ser80. For example, introduction of a *cis*-peptidyl-Pro bond at positions 18–19, believed to be caused by introduction of a Pro at position 19 was found to favour domain swapping [47]. However, mutation of Ala19 to Pro in RNase A leads to a decrease in dimer formation [47]. Thus, the destabilization of

the peptide segment 1–20 does not lead on its own to the BS-RNase dimer formation, but together with the introduction of two cysteines at positions 31 and 32 and a leucine residue at position 28 [21] facilitates the swapping of this segment, the formation of the interchain disulphide bonds and the dimerization. Also, given the different RNase dimers observed in crystal structures, the nature of the dimer interface is also important for the correct association of the dimers and this can probably assign some importance in substitutions affecting the surface of the molecule. Furthermore, different surface charges can help intersubunit adhesion in a certain way which will lead to the formation of active dimers and prevent accidental adhesion, which leads to the formation of inactive dimers.

Our structural results could provide an insight into the increased catalytic activity observed against duplex RNA with RNase variants carrying a Gly at position 111. The increased flexibility in the loop containing residues 111–115 following this substitution may permit the protein to better accommodate the duplex RNA in the 'two sites' model outlined by Opitz *et al*. [22]. In this model, each of the two active sites of BS-RNase cleaves 5′ phosphodiester bonds, which are in different strands of the double-stranded RNA. This requires an almost 90° bend of the oligonucleotide chain, which wraps around the dimer. Residues 111 and 38 are at either end of the two active sites (Fig. 1B). In the crystal structure of the RNase A, d(ApTpApApG) [48], which was the basis for the 'two sites' model, the side chain of Glu111 is 3.4–3.9 Å array from the two adenosines in the 5′ end, and is involved in van der Waals interactions with the adenine rings. Thus, the change from Glu to Gly in position 111 and the loss of a negative charge in this position might help the RNA molecule to adopt the 90° bend required in the 'two-site' model and to wrap around better. Interestingly, in the 'two-site' model, the duplex RNA is not obliged to pass near the remainder of the basic surface, possibly explaining why the remainder of the basic surface has little impact on the ability of the RNA to hydrolyse duplex RNA.

ACKNOWLEDGEMENTS

We are grateful to the staff at the Synchrotron Radiation Source, Daresbury, UK, and to Dr Anastassios Papageorgiou for help with X-ray data collection. This work is supported by the Medical Research Council (U.K.) and the Wellcome Trust (U.K.) equipment grant (K.R.A.), the Swiss National Foundation, Sandoz AG and the Swiss Federal Institute of Technology (S.A.B.).

REFERENCES

1. Beintema, J.J., Schuller, C., Irie, M. & Carsana, A. (1988) Molecular evolution of the ribonuclease superfamily. *Prog. Biophys.* **51**, 165–192.
2. Trabesinger-Rüf, N., Jermann, T.M., Zankel, T.R., Durrant, B., Frank, G. & Benner, S.A. (1996) Pseudogenes in ribonuclease evolution. A source of new biomacromolecular function? *FEBS Lett.* **382**, 319–322.
3. Fett, J.W., Strydom, D.J., Lobb, R.R., Alderman, E.M., Bethune, J.L., Riordan, J.F. & Vallee, B.L. (1985) Isolation and characterization of angiogenin, an angiogenic protein from human carcinoma-cells. *Biochemistry* **24**, 5480–5486.
4. Strydom, D.J., Fett, J.W., Lobb, R.R., Alderman, E.M., Bethune, J.L., Riordan, J.F. & Vallee, B.L. (1985) Amino-acid sequence of human tumor derived angiogenin, *Biochemistry* **24**, 5486–5494.
5. Gleich, G.J., Loegering, D.A., Bell, M.P., Checkel, J.L., Ackerman, S.J. & McKean, D.J. (1986) Biochemical and functional similarities between human eosinophil derived neurotoxin and eosinophil cationic protein—homology with ribonuclease. *Proc. Natl Acad. Sci. USA* **83**, 3146–3150.
6. Rosenberg, H.F., Tenen, D.G. & Ackerman, S.J. (1989) Molecular-cloning of the human eosinophil-derived neurotoxin—a member of the ribonuclease gene family. *Proc. Natl Acad. Sci. USA* **86**, 4460–4464.
7. Ardelt, W., Mikulski, S.M. & Shogen, K. (1991) Amino-acid sequence of an antitumour protein from Rana-Pipiens oocytes and early embryos – homology to pancreatic Ribonucleases. *J. Biol. Chem.* **266**, 245–251.
8. Okabe, Y., Katayama, N., Iwama, M., Watanabe, H., Ohgi, K., Irie, M., Nitta, K., Kawauchi, H., Takayanagi, Y., Oyama, F., Titani, K., Abe, Y., Okazaki, T., Inokichi, N. & Koyama, T. (1991) Comparative base specificity, stability, and lectin activity of 2 lectins from eggs of *Rana-Catesbeiana* and *R-Japonica* and liver ribonuclease from *R-Catesbeiana*. *J. Biochem.* **109**, 786–790.
9. Breukelman, H.J., Beintema, J., .J., Confalone, E., Costanzo, C., Sasso, M.P., Carsana, A., Palmieri, M. & Furia, A. (1993) Sequences related to the ox pancreatic ribonuclease coding region in the genomic DNA of mammalian-species. *J. Mol. Evol.* **37**, 29–35.
10. D'Alessio, G., Di Donato, A. & Parente, A. (1991) Seminal RNase – A unique member of the ribonuclease superfamily. *Trends Biochem. Sci.* **16**, 104–106.
11. Matoušek, J. (1973) The effect of bovine seminal ribonuclease (BS RNase) on cells of crocker tumours in mice. *Experientia* **29**, 858–859.
12. Vescia, S. & Tramontano, D. (1981) Anti-tumoral action of bovine seminal ribonuclease – definition of experimental parameters. *Mol. Cell. Biochem.* **36**, 125–128.
13. Soucek, J., Matousek, J., Chudomel, V. & Lindnerova, G. (1981) Inhibitory effect of bovine seminal ribonuclease on activated lymphocytes lymphoblastoid cell-lines *in vitro*. *Folia Biol.* **27**, 334–345.
14. Soucek, J., Hruba, A., Paluska, E., Chudomel, V., Dostal, J. & Matousek, J. (1983) Immunosuppressive effects of bovine seminal fluid fractions with ribonuclease-activity. *Folia Biol.* **29**, 250–261.
15. Soucek, J., Chudomel, V., Potmesilova, I. & Novak, J.T. (1986) Effect of ribonucleases on cell-mediated lympholysis reaction and on Gm-Cfc colonies in bone-marrow culture. *Nat. Immun. Cell Growth Regul.* **5**, 250–258.
16. Dostàl, J. & Matoušek, J. (1973) Isolation and some chemical properties of aspermatogenic substance from bull seminal vesicle fluid. *J. Reprod Fertil.* **33**, 263–274.
17. Capasso, S., Giordano, F., Mattia, C.A., Mazzarella, L. & Zagari, A. (1983) Refinement of the structure of bovine seminal ribonuclease. *Biopolymers* **22**, 327–332.
18. Mazzarella, L., Capasso, S., Demasi, D., Di'Lorenzo, G., Mattia, C.A. & Zagari, A. (1993) Bovine seminal ribonuclease – structure at 1.9 Å resolution. *Acta Crystallogr.* **D49**, 389–402.
19. Di Donato, A., Cafaro, V., Romeo, I. & D'Alessio, G. (1995) Hints on the evolutionarry design of a dimeric RNase with special bioactions. *Protein Sci.* **4**, 1470–1477.
20. Mazzarella, L., Vitagliano, L. & Zagari, A. (1995) Swapping structural determinants of ribonuclease: an energetic analysis of the hinge peptide 16–22. *Proc. Natl Acad. Sci. USA* **92**, 3799–3803.
21. Ciglic, M.I., Jackson, P.J., Raillard, S.A., Haugg, M., Jermann, T.M., Opitz, J.G., Trabesinger-Ruf, N. & Benner, S.A. (1998) Origin of dimeric structure in the ribonuclease superfamily. *Biochemistry* **37**, 4008–4022.
22. Opitz, J.G., Ciglic, M.I., Haugg, M., Trautwein-Fritz, K., Raillard, S.A., Jermann, T.M. & Benner, S.A. (1998) Origin of the catalytic activity of bovine seminal ribonuclease against double-stranded RNA. *Biochemistry* **37**, 4023–4033.
23. Kim, J.S., Soucek, J., Matousek, J. & Raines, R.T. (1995) Catalytic activity of bovine seminal ribonuclease is essential for its immunosuppressive and other biological activities. *Biochem. J.* **308**, 547–550.
24. D'Alessio, G., DiDonato, A., Parente, A. & Piccoli, R. (1991) Seminal RNase – A unique member of the ribonuclease superfamily. *Trends Biochem. Sci.* **16**, 104–106.
25. Nambiar, K.P., Stackhouse, J., Stauffer, D.M., Kennedy, W.G., Eldredge, J.K. & Benner, S.A. (1984) Total synthesis and cloning of a gene coding for the ribonuclease-S protein. *Science* **223**, 1299–12301.

26. Yanisch-Perron, C., Vieira, J. & Messing, J. (1985) Improved M13 phage cloning and host strains- nucleotide sequences of the M13MP18 and PUC19 vector. *Gene* **33**, 103–119.
27. McGeehan, G.M. & Benner, S.A. (1989) An improved system for expressing pancreatic ribonuclease in *Escherichia coli*. *FEBS Lett.* **247**, 55–56.
28. Trautwein, K.P., Holliger, P., Stackhouse, J. & Benner, S.A. (1991) Site-directed mutagenesis of bovine pancreatic ribonuclease: lysine-41 and aspartate-121. *FEBS Lett.* **281**, 275–277.
29. Leonidas, D.D., Shapiro, R., Irons, L.I., Russo, N. & Acharya, K.R. (1997) Crystal structures of ribonuclease A complexes with 5′-diphosphoadenosine 3′-phosphate and 5′-diphosphoadenosine 2′-phosphate at 1.7 Å resolution. *Biochemistry* **36**, 5578–5588.
30. Otwinowski, Z. & Minor, W. (1997) In: *Methods in Enzymology*, Vol. 276 (Carter, C.W.J. & Sweet, R.M., eds), pp. 307–326. Academic Press, New York.
31. Kabsch, W. (1988) Evaluation of single crystal X-ray diffraction data from a position sensitive detector. *J. Appl. Crystallogr.* **21**, 916–924.
32. C.C.P.4 (1994) The CCP4 suite: programs for protein crystallography. *Acta Crystallogr.* **D50**, 760–763.
33. French, S. & Wilson, K.S. (1978) On the treatment of the negative intensity observations. *Acta Crystallog.* **A34**, 517–525.
34. Navaza, J. (1994) AMoRe: an automated package for molecular replacement. *Acta Crystallog.* **A50**, 157–163.
35. Howlin, B., Moss, D.S. & Harris, G.W. (1989) Segmented anisotropic refinement of bovine ribonuclease A by the application of rigid-body tls model. *Acta Crystallogr.* **A45**, 851–861.
36. Brünger, A.T. (1992) *X-PLOR Version 3.1 Manual: A System for X-ray Crystallography and NMR*. Yale University Press, New Haven, CT, USA.
37. Brünger, A.T. (1992) Free R value: a novel statistical quantity for assessing the accuracy of crystal structures. *Nature* **355**, 472–475.
38. Jiang, J.-S. & Brünger, A.T. (1994) Protein hydration observed by X-ray diffraction: solvation properties penicillopepsin and neuraminidase crystal structures. *J. Mol. Biol.* **243**, 100–115.
39. Read, J. (1986) Improved Fourier coefficient for maps using phases from partial structures with errors. *Acta Crystallogr.* **A42**, 140–149.
40. Laskowski, R.A., MacArthur, M.W., Moss, D.S. & Thornton, J.M. (1993) PROCHECK – A program to check the stereochemical quality of protein structures. *J. Appl. Crystallogr.* **26**, 283–291.
41. Kraulis, P.J. (1991) MOLSCRIPT – A program to produce both detailed and schematic plots of protein structures. *J. Appl. Crystallogr.* **24**, 946–950.
42. Esnouf, R.M. (1997) An extensively modified, version of Molscript that includes greatly enhanced coloring capabilities. *J. Mol. Graphics Modelling* **15**, 132–134.
43. Stuart, D.I., Levine, M., Muirhead, H. & Stammers, D.K. (1979) The catalytic structure of cat pyruvate kinase at a resolution of 2.6 Å. *J. Mol. Biol.* **134**, 109–142.
44. Nicholls, A. & Honig, B. (1991) A rapid finite difference algorithm, utilising successive over relaxation to solve the Poisson-Boltzmann equation. *J. Comput. Chem.* **12**, 435–445.
45. Liu, Y., Hart, P.J., Schlunegger, M.P. & Eisenberg, D. (1998) The crystal structure of a 3D domain-swapped dimer of RNase A at a 2.1 Å resolution. *Proc. Natl Acad. Sci. USA* **95**, 3437–3442.
46. Richards, F.M. & Wyckoff, H.W. (1971) Bovine pancreatic ribonuclease. *Enzymes* **4**, 647–806.
47. Parente, A. & D'Alessio, G. (1985) Reacquisition of quaternary structure by fully reduced and denatured seminal ribonuclease. *Eur. J. Biochem.* **149**, 381–387.
48. de Fontecilla-Camps, J.C., Llorens, R., le Du, M.H. & Cuchillo, C.M. (1994) Crystal structure of ribonuclease A·d(ApTpApApG) complex. *J. Biol. Chem.* **269**, 21526–21531.